Macromolecules

ARTICLE

pubs.acs.org/Macromolecules

A Simple Method for Obtaining the Information of Orientation Distribution Using Polarized Raman Spectroscopy: Orientation Study of Structural Units in Poly(lactic acid)

Min Sang Park,[†] Yee Shan Wong,[§] Jung Ok Park,[†] Subbu S. Venkatraman,*[,§] and Mohan Srinivasarao*[,†,‡]

[†]School of Materials Science and Engineering and [‡]School of Chemistry and Biochemistry, Georgia Institute of Technology, Atlanta, Georgia 30332, United States

[§]School of Materials Science and Engineering, Nanyang Technological University, Singapore 639798, Singapore

Supporting Information

ABSTRACT: A simple approach using polarized Raman spectroscopy has been employed to study the molecular orientation distribution in both the crystalline and amorphous regions of uniaxially oriented poly(L-lactic acid) (PLLA) films. The effect of morphology on the intensity of the Raman bands was evaluated to provide qualitative information on the distributions of the crystalline and amorphous regions to the peak intensities. The angular dependence of the scattered intensity of assignable vibration bands was analyzed to quantify the orientation degree of the symmetry axis of Raman tensors. The results showed that the measurement of polarization of scattered intensity as a function of rotating angle can provide semiqualitative information on the shape of the orientation distribution function. On the basis of the results, orientational variation of both amorphous and crystalline chains can be described under the deformation of film and compared with previous studies.

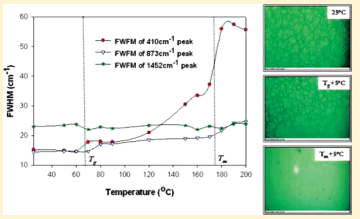

1. INTRODUCTION

Semicrystalline lactic acid-based aliphatic polyester (PLLA) has been used as a biomaterial because the polymer and its degradation products have been found to be acceptable from a biocompatibility standpoint in various applications.[1,2] The physical properties of PLLA have been extensively studied by various research groups; it is well-known that the macroscopic physical properties such as mechanical strength, thermal stability,[3,4] and degradation kinetics[5] depend on its microscopic structure such as the crystal structure and molecular orientation.[6−8]

Molecular orientation is known to play a significant role in determining mechanical performance of drawn polymer films and fibers. Semicrystalline PLLA is essentially composed of alternating crystalline and amorphous regions which respond differently at the structural level to macroscopic deformation. This difference is critical in physical properties because there is such a large change between external forces involved in bond stretching and bending as well as other modes of deformation.[9,10]

Our interest in orientation effects in these polymers stems from the development of shape-memory based medical devices.[11] We are particularly interested in understanding the advantages and limitations of this class of biodegradable polyesters in shape memory applications, as parts of implanted devices such as coronary stents.[11,12] For such applications, the polymer is shaped into a tubular construct, and then shape memory is incorporated into it in order to facilitate its development in the body. Although cross-linked polymers are ideal for this sort of device, we have shown that un-cross-linked polymers may also be programmed to exhibit adequate shape memory effects.[13] However, the details of the changes of orientation with shape deformation history have not been studied. Thus, characterization of orientation of polymer chains in crystalline and especially amorphous region is necessary so that physical properties of the products may be more fully understood and usefully modified.

While diffraction methods such as X-ray diffraction are capable of elucidating the crystalline structure, few deterministic methods allow us to describe the transformation of an isotropic to anisotropic amorphous polymer chains in semicrystalline polymer due to the complex conformation and absence of long-range coherence. Vibrational spectroscopy, however, is informative in providing valuable orientation properties of amorphous polymer chains in that they enable the detection of localized structures at the molecular scale and the separation of vibration of polymer chains in amorphous region from those of the crystalline region.[14,15]

Since the first application of polarized Raman spectroscopy to establish the quantitative relationship between polarization intensity and the molecular orientation in a polymeric system was developed by Bower,[16] there have been numbers of studies analyzing molecular orientation of several semicrystalline polymers.[17−19] Recently, Tanaka et al. have introduced a good way to use polarized Raman spectroscopy for obtaining the degree of molecular orientation between the amorphous and crystalline regions in semicrystalline polymers[20,21] including

Received: July 11, 2010
Revised: January 31, 2011
Published: March 07, 2011

PLLA.[22] In their publications, they reported a methodology for separating the degree of orientation of polymer chains in the amorphous and crystalline regions by combining $\langle P_{400} \rangle$ and $\langle P_{200} \rangle$ for the cylindrical symmetry axis of Raman tensor with orientation information from XRD and birefringence techniques.

In this study, we will expand the way of using polarized Raman spectroscopy to quantify the degree of orientation of structural units in semicrystalline polymer, PLLA, as well as to obtain qualitative information about responsive behaviors of both amorphous and crystalline chains with quite different approaches. Rather than simply reproducing the orientation degrees in both crystalline and amorphous chains, the present work aims at shedding light on the coupling between the analysis of the anisotropy of polarization intensities of various vibrational modes and deformation histories of molecules.

2. FUNDAMENTAL INFORMATION

2.1. Polarization of Raman Scattering and Directional Information. Spectroscopy such as polarized Raman or polarized infrared that uses vibrational modes of the system can potentially provide a great deal of information about orientation distribution of molecules in both crystalline and amorphous regions since crystallinity affects these transitions and can be separated from amorphous peaks.[14]

The difference between these two methods arises from the fundamentally different processes involved in the generation of the spectra as well as selection rules[14,23] to determine whether the vibration is active in the IR and Raman spectra. Polarized infrared spectroscopy involves only one beam of polarized radiation, and the fraction of the radiation absorbed by a single molecule depends only on the orientation of the molecule with respect to the polarization vector of the incident radiation. The intensity of polarized Raman scattering, in contrast, depends on the orientation of the molecule with respect to two polarization vectors of incident beam and beam scattered by a molecule. This means that polarized Raman spectroscopy can in principle yield more information about the distribution of orientations of molecules.

When a molecule is placed in an electric field, **E**, it suffers distortions which produces an induced dipole moment, **P**, given by $\mathbf{P} = \boldsymbol{\alpha}\mathbf{E}$. In actual molecular systems, both **P** and **E** are vectors consisting of three components in the *x*, *y*, and *z* directions. Thus, induced dipole moment, **P**, can be written in matrix form as

$$\begin{bmatrix} P_x \\ P_y \\ P_z \end{bmatrix} = \begin{bmatrix} \alpha_{xx} & \alpha_{xy} & \alpha_{xz} \\ \alpha_{yx} & \alpha_{yy} & \alpha_{yz} \\ \alpha_{zx} & \alpha_{zy} & \alpha_{zz} \end{bmatrix} \begin{bmatrix} E_x \\ E_y \\ E_z \end{bmatrix} \quad (1)$$

The first matrix of the right-hand side is called the polarizability tensor.[23] Raman scattering occurs with a change in vibrational energy of molecules if one of these components of the polarizability tensor is changed by the displacement of the *k*th atom, q_k, during the vibration. Hence, Raman scattering is related to the rate of change of polarizability, $\alpha' = \partial\alpha/\partial q_k$, which is one of the tensorial components called a Raman tensor.[16,23,24]

In anisotropic materials where orientations of molecules are not distributed uniformly, the anisotropic nature of Raman tensor is capable of providing information on any ordering in the oriented system. It can be described by measuring polarized Raman intensities. As briefly explained earlier, when incident light consisting of the vibration of an electromagnetic wave encounters a substance, the light interacts with the atoms and induces a change in polarizability. The degree of the polarizability change depends on the angle between the electric vector of the incident light and the symmetry axes of Raman tensor, which can thus provide directional information about the distribution of the symmetry of Raman tensor. In this point of view, light without a specific electric vector is not suitable to obtain such information since there is no preferential direction of the electric field vector and interference may occur in any direction.When polarized light is incident on a single scattering unit, the analyzed Raman intensities at various vibration modes depend on the angles between the electric vector of the incident/scattered light and the symmetry axes of the Raman tensors as well as the magnitude of Raman tensor itself. As a result, the amplitude transmitted by analyzer is determined by the combination of polarization of incident and scattered light and can be expressed by[16,23]

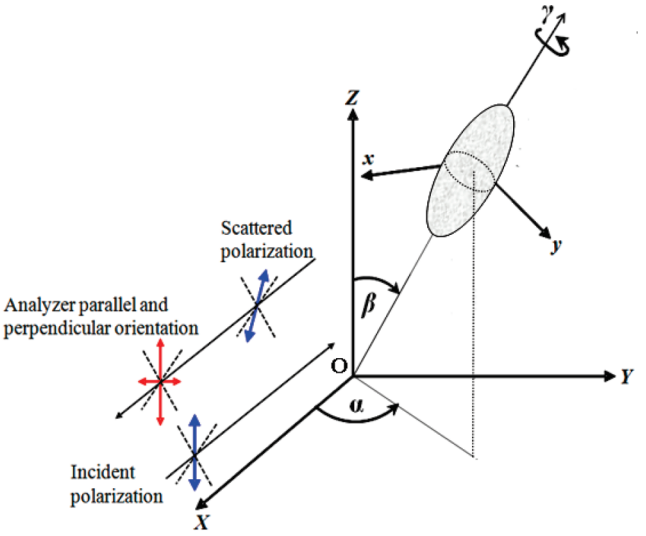

Figure 1. Euler angles, α, β, γ are defined with principal axes of Raman tensor, *O-xyz*, in a macroscopic (laboratory) system of axes, *O-XYZ*. The polarization of the Raman scattered light is resolved onto the different direction of analyzer.

$$I_s = k\sum(\sum_{ij} E_i \alpha'_{ij} E_j)^2 \quad (2)$$

where E_j is the directional cosine of the incident electric polarization vector and E_i is the directional cosine of the scattered electric polarization vector. *k* is a proportionality constant taking account of experimental factors such as incident light intensity, instrumental transmission, light collection efficiency, etc. It is, therefore, possible to determine the oriented direction of symmetry axis of Raman tensor using information about direction cosine of incident and scattered polarization.

2.2. Orientation Distribution Function. In general, the orientation information on scattering units can be described by means of the orientation distribution function (ODF), which can be expanded in a series of generalized spherical harmonics.[25,26] Figure 1 shows the geometry where the scattering unit orients to a specific direction in a given system, which can be described in terms of Euler angle (α, β, γ). It may be shown that, whether a scattering unit has any symmetrical elements or not, it is always possible to find a set of three mutually perpendicular axes *O-xyz*.[27] Rotating the scattering unit through 180° about any one of

these axes does not change the distribution of orientation with respect to a fixed observer.

Using this idea of principal axes, one can look for a set of orthogonal functions of Euler angle (α, β, γ) that can be used to construct a simple ODF expansion. For these orthogonal functions, we can make a use of the elements of the Wigner rotation matrices. This will enable us to transform the orientation dependence of physical quantities in the macroscopic (or laboratory) frame of reference *O-XYZ* to their orientation dependence in the scattering unit frame, *O-xyz*. The ODF is generally expressed as[28,29]

$$f(\alpha,\beta,\gamma) = \sum_{L=0}^{\infty} \sum_{m,n=-L}^{L} \frac{2L+1}{8\pi^2} \langle D_{mn}^{L*} \rangle D_{mn}^{L}(\alpha,\beta,\gamma) \quad (3)$$

where $D_{mn}^{L}(\alpha,\beta,\gamma)$ are the Wigner rotation matrices and $\langle D_{mn}^{L} \rangle$ indicates the statistical average of $D_{mn}^{L}(\alpha,\beta,\gamma)$. Depending on the values of L ($L \in N$), the ODF is composed of a set of $(2L+1)^2$ Wigner matrices.[28] Since the study of polarized Raman spectroscopy allows us to obtain information about the cosine direction up to fourth rank, the expansion of eq 3 is allowed up to $L = 4$. Furthermore, if there are certain symmetries in both the sample and scattering units, a number of components are left out of consideration so that ODF can be simplified.[16,30] The simplest ODF is for the case of cylindrical symmetry. It is usually assumed that the distribution of scattering units will be random with rotation about the Euler angle α and γ, and as a result, the ODF is simplified to be a 1-dimensional function depending on only polar angle β. In this case, the expansion coefficients $\langle D_{mn}^{L} \rangle$ only have values other than zero when $m = 0$ and $n = 0$, and we can expand this matrix in terms of the series of Legendre polynomials, $\langle P_{L00} \rangle$.

As a result of simplicity, the ODF can be expressed by $f(\beta)$ as

$$f(\beta) = \frac{1}{8\pi^2}\left\{1 + \frac{5}{2}\langle P_{200}\rangle(3\cos^2\beta - 1) + \frac{9}{8}\langle P_{400}\rangle(3 - 30\cos^2\beta + 35\cos^4\beta)\right\} \quad (4)$$

The expansion coefficients, $\langle P_{200} \rangle$ and $\langle P_{400} \rangle$, are called orientation order parameters and are calculated from the orthogonality of Legendre polynomials as

$$\langle P_{200} \rangle = \frac{1}{2}\int_0^{\pi} P_{200} f(\beta) \sin\beta \, d\beta = \frac{1}{2}(3\langle \cos^2\beta \rangle - 1) \quad (5)$$

$$\langle P_{400} \rangle = \frac{9}{8}\int_0^{\pi} P_{400} f(\beta) \sin\beta \, d\beta = \frac{1}{8}(3 - 30\langle \cos^2\beta \rangle + 35\langle \cos^4\beta \rangle) \quad (6)$$

In the study of multiunits which are 3-dimensionally distributed in a system, it is necessary to consider the orientation distribution of scattering units on deriving the equation of statistically averaged polarized Raman intensities. So, the measured intensity of scattered light includes quantities of scattering units that contain information about the distribution of orientation. Therefore, eq 2 should be derived considering orientation distribution of the scattering units integrated over all possible orientations as

$$I_{ij}(\theta) = k{\alpha'}_{ij}^{2} \int_{\beta}\int_{\alpha}\int_{\gamma} f(\alpha,\beta,\gamma)(E_{ij}(\alpha,\beta,\gamma,\theta))^2 \, d\gamma \, d\alpha \sin\beta \, d\beta \quad (7)$$

where E_{ij} is the electric field equations with rotational degree of freedom. θ is the angle between the incident polarization direction and the symmetry axis of Raman tensor. The notation I_{ij} denotes the scattering intensity analyzed in i direction (in our geometry, $i \equiv Z, Y$) with incident polarization in j direction (in our geometry, $j \equiv Z, Y$).

2.3. Symmetry of Raman Tensor and Depolarization Ratio. As shown in eq 7, it must be emphasized that principal components of Raman tensor are of prime importance in determining the directional relationship between scattering units and **E**.[27] In dealing with the orientation distribution of Raman tensor axes in a multiunits system, there has been an ambiguity in the choice of α and γ angle dependences of principal components (i.e., $a \neq b$ in eq 8), and this is associated with questions concerning the assumption of local cylindrical symmetry (i.e., $a = b$) of the Raman tensor.[29]

$$\alpha' = \begin{pmatrix} a & 0 & 0 \\ 0 & b & 0 \\ 0 & 0 & c \end{pmatrix} \quad (8)$$

Discussion about the importance of deviation of cylindrical symmetry in Raman tensor axes was made by Jen et al.,[29] and they showed the insensitivity of uniaxial orientation order parameters of main principal axis ($c, c \gg a, b$) of Raman tensor, i.e., $\langle P_{200} \rangle$ and $\langle P_{400} \rangle$. Thus, in this study, we will obtain $\langle P_{200} \rangle$ and $\langle P_{400} \rangle$ values for orientation degree of the principal axis of Raman tensor in stretched samples without considering the expansion coefficients of ODF related to biaxial symmetry of Raman tensor (i.e., the cases of nonzero m and n in Wigner rotation matrix). It should, however, be noticed that this does not necessarily mean that all Raman bands possess tensor forms with cylindrical symmetry, while it does mean that ignoring the biaxial terms in ODF may not significantly affect $\langle P_{200} \rangle$ and $\langle P_{400} \rangle$ values. Accordingly, we will identify the anisotropic distribution of the principal axis of Raman tensor with respect to the drawing direction (director) considering only β angle dependence and thus nontrivial order parameters, $\langle P_{200} \rangle$ and $\langle P_{400} \rangle$, characterizing the "axial" ordering of principal axis of Raman tensor in stretched films.

For any Raman-active mode, the values of the tensor components depend on the choice of coordinate system, and several choices of coordinate systems leading to an especially simple tensor form are described in detail elsewhere.[27] Suffice it to say that the pattern of entries in a tensor is essential for analyzing the orientation distribution of Raman tensor axes. Valuable information about the symmetry of Raman tensor can be obtained by measuring depolarization ratio of polarized Raman intensity in the isotropic state, R_{iso}. The depolarization ratio is indispensable in making band assignments for studying the orientation distribution of scattering units and is defined by[16,23,27]

$$R = \frac{I_{\perp}}{I_{\parallel}} = \frac{3\xi^2}{10\delta^2 + 4\xi^2} \quad (9)$$

where $I_{\perp}$ and $I_{\parallel}$ represent the Raman scattering intensities when the polarization direction of analyzer is perpendicular and parallel to that of the incident beam, respectively. δ^2 is the isotropic part of the tensor, and ξ^2 is the anisotropic part. These quantities are defined in terms of the components of the Raman tensor as

$$\delta^2 = \frac{1}{3}(\alpha'_{xx} + \alpha'_{yy} + \alpha'_{zz})^2 \quad (10)$$

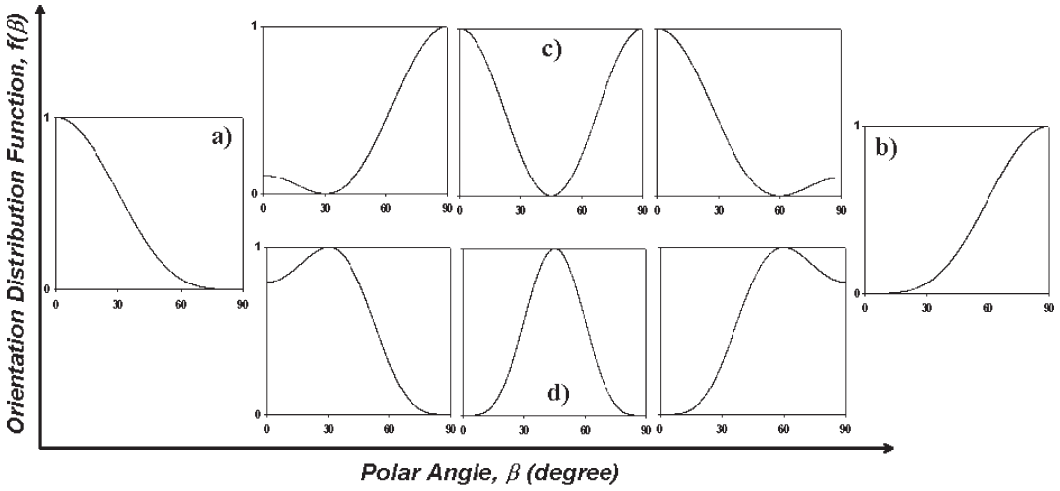

Figure 2. Different types of orientation distribution functions of polymer chain corresponding to the equation of Nomura et al.:[40] (a) monotonic decrease with a single maximum at $\beta = 0°$, (b) monotonic increase with a single maximum at $\beta = 90°$, (c) bimodal function with a single minimum at specific angle, (d) unimodal function with a single maximum at specific angle.

$$\xi^2 = \frac{1}{3}[(\alpha'_{xx} - \alpha'_{yy})^2 + (\alpha'_{xx} - \alpha'_{zz})^2 + (\alpha'_{yy} - \alpha'_{zz})^2] + \frac{1}{2}[(\alpha'_{xy} + \alpha'_{yx})^2 + (\alpha'_{xz} + \alpha'_{zx})^2 + (\alpha'_{yz} + \alpha'_{zy})^2] \quad (11)$$

The values of δ^2 and ξ^2 depend on the Raman tensor components, and so measurement of R_{iso} can in principle give symmetry information on Raman tensor in spite of the random molecular orientation. Conventionally, Raman tensor is said to be symmetric (polarized) and have only diagonal components when $0 < R_{iso} < {}^3/_4$ and to be nonsymmetric (depolarized) and have off-diagonal components when $R_{iso} = {}^3/_4$.[23,31] From the measurements of R_{iso}, therefore, it is possible to exploit Raman bands possessing simple symmetric tensor form. Nevertheless, theoretically, an interpretation of the peak intensities (eq 7) in terms of $\langle\cos^2\beta\rangle$ and $\langle\cos^4\beta\rangle$ is not easy because it requires knowledge of the principal components of the Raman tensor which are quite complicated to obtain. However, using the depolarization ratio, R, we can calculate these coefficients without knowing their exact values. In addition, one can eliminate the proportionality effect, k, which can be affected by experimental error or laser instability by defining the depolarization ratio.

In many studies in the literature,[22,32−34] depolarization ratios with specific geometries, $R_1 = I_\perp/I_\parallel$ ($\theta = 0°$) and $R_2 = I_\perp/I_\parallel$ ($\theta = 90°$), were measured, which made it possible to solve for the two unknown coefficients, $\langle P_{200}\rangle$ and $\langle P_{400}\rangle$. The value of $r = \alpha'_{yy}/\alpha'_{zz}$ is solved from the value of depolarization ratio at random orientation state, R_{iso}.

$$R_{iso} = \frac{(1-r)^2}{3 + 4r + 8r^2} \quad (12)$$

This methodology has been applied satisfactorily for the measurement of orientation distribution of various polymer chains.[17,34,35] However, from the fact that r value may not be constant when molecules are under the stress,[27] it should be treated as a variable according to the deformation.

In this work, depolarization ratio profile over the entire range of 0−360° will be analyzed in order to obtain more accurate orientation properties, which provides more directional information on the principal axis of Raman bands than only parallel and perpendicular polarization of laser excitation.[36,37] Orientation order parameters, $\langle P_{200}\rangle$ and $\langle P_{400}\rangle$, and r value are calculated by fitting measured depolarization ratio profile to the equation of $R(\theta)$ which is derived from eq 7 instead of deducing from only R_1 and R_2 values.

$$R(\theta) = \frac{I_\perp(\theta)}{I_\parallel(\theta)} = \frac{I_{YZ}(\theta)}{I_{ZZ}(\theta)} = \{(-1+r)^2[-56 - 40\langle P_{200}\rangle + (105\cos 4\theta - 9)\langle P_{400}\rangle]\}/\{-56(8r^2 + 4r + 3) + 40(4r^2 - r - 3)(1 + 3\cos 2\theta)\langle P_{200}\rangle - 3(r-1)^2(9 + 20\cos 2\theta + 35\cos 4\theta)\langle P_{400}\rangle\} \quad (13)$$

2.4. Mutually Consistent Values of $\langle P_{200}\rangle$ and $\langle P_{400}\rangle$. In the case of polymer chains, the orientation distribution does not necessarily occur with a monotonic pattern but can have more complicated patterns. Nomura et al.[38] and Bower et al.[39] showed the graphical representation of the state of orientation in polymer system using plots of $\langle P_{400}\rangle$ against $\langle P_{200}\rangle$ for several types of distribution under uniaxial deformation. They simulated the mutual relations between $\langle P_{200}\rangle$ and $\langle P_{400}\rangle$ when determined from the boundary equations of trigonometric functions. Using the relationship between $\langle\cos^2\beta\rangle$ and $\langle\cos^4\beta\rangle$ by the Schwarz inequality, the variation of $\langle P_{400}\rangle$ should be in the limited area of the following formula if $\langle P_{200}\rangle$ value is known:[38,40]

$$\frac{1}{18}(35\langle P_{200}\rangle^2 - 10\langle P_{200}\rangle - 7) \le \langle P_{400}\rangle \le \frac{1}{12}(5\langle P_{200}\rangle + 7) \quad (14)$$

In their graphical representations, there are four types of orientation distribution functions: monotonically increasing or decreasing function which has a single maximum at $\beta = 0°$ or 90°, respectively, unimodal function which has a maximum at specific angle except at $\beta = 0°$ and 90°, and bimodal function which has two maximum peak at $\beta = 0°$ and 90° and one minimum at specific angle. Each of the orientation models is illustrated in Figure 2, and the domain of the variation of $\langle P_{200}\rangle$ against $\langle P_{400}\rangle$ for each model is depicted in Figure 3. Model I represents a monotonic decrease of the orientation distribution function $f(\beta)$

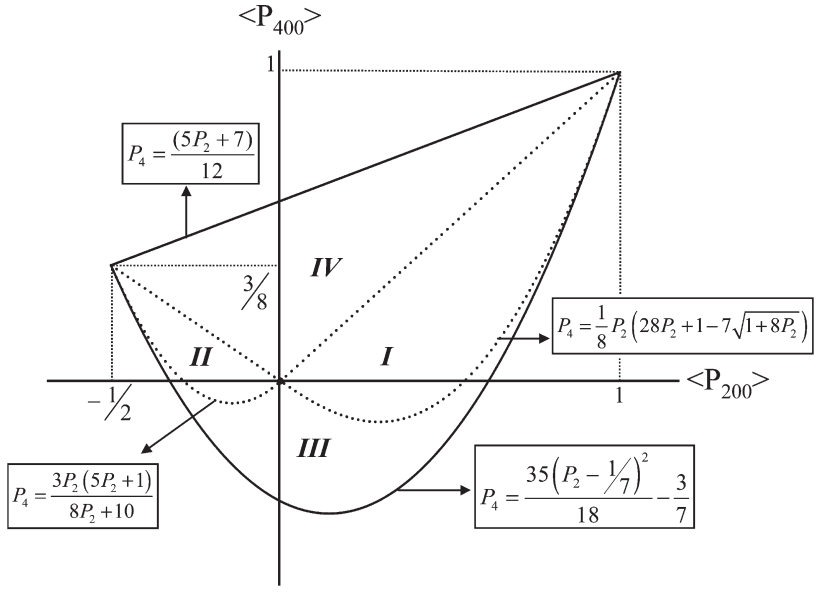

Figure 3. Possible four planes for the relation of $\langle P_{200}\rangle$ and $\langle P_{400}\rangle$ according to the types of ODF; solid line is bounds on the mutually consistent values of $\langle P_{200}\rangle$ and $\langle P_{400}\rangle$; dashed lines are plotted to divide the $\langle P_{200}\rangle$ and $\langle P_{400}\rangle$ planes according to types of ODF.[39]

with increasing β, while model II represents a monotonic increase of the population with increasing β. For model III, the function $f(\beta)$ has at least one maximum at β where $0° < \beta < 90°$, and the function $f(\beta)$ has at least one minimum at β where $0° < \beta < 90°$ for model IV. By comparing the obtained values of $\langle P_{200}\rangle$ and $\langle P_{400}\rangle$ with four domains in Figure 3, we can predict a type of orientation distribution of polymer chains in a system.

3. EXPERIMENTAL SECTION

3.1. Sample Preparation. Poly(L-lactide) (PLLA) ($M_w = 1.9 \times 10^6$) was purchased from Purac Biochem and was used as received. Film specimens were prepared by casting from an isotropic solution of PLLA in dichloromethane. Solutions were cast onto glass plates using an automatic film applicator. The solvent evaporated, and films with a uniform thickness of 0.1 mm were obtained. Some degree of uniaxial orientation could be achieved by drawing the solution cast film at 85 °C and then quenching to room temperature. The crosshead speed of the machine was 10 mm/min.

Macroscopic uniaxial orientation in stretched films was observed by polarized optical microscope (POM). Under crossed polarization, optical microscopic images of stretched films appeared with 2-fold rotational symmetry of sample in birefringence. When drawing direction is parallel or perpendicular to polarization direction of incident light, it became dark, while the maximum intensity of transmitted light was obtained when rotating the drawing direction is 45° with respect to the polarization direction of incident light. This indicates that polymer chains in stretched films are aligned uniaxially on a macroscopic scale.[41,42] Another evidence of the uniaxial nature of the sample comes from wide-angle X-ray diffraction (WAXRD) data shown in the Supporting Information. Neither method showed any preferred orientation around the draw direction, thus confirming uniaxial orientation for the stretched films.

For the determination of R_{iso} values for the Raman bands of PLLA, an isotropic crystalline film with 30% crystallinity was obtained by cooling the melted PLLA until the temperature fell to room temperature (at 20 °C/h).

3.2. Experimental Setup and Spectra Analysis. The polarized Raman spectra were obtained using 10× objective and a 785 nm laser light source (Kaiser Optic System) which has 4 cm^{-1} resolution in backscattering geometry as depicted in Figure 1. The polarized component, $I_{\parallel}$, was obtained by setting the analyzer polarization parallel to the polarization direction of the incident beam while the depolarized component, $I_{\perp}$, was resolved by setting the polarization of the analyzer perpendicular to that of the incident beam.

In order to obtain any combination of angle of polarization vectors of incident light (θ) against principal axis of Raman tensor, we rotated the sample stage against polarization direction of the incident beam. Detailed analysis of the orientation in terms of incident polarization vector was performed by recording a series of spectra over the entire range of 0−360° at 10° intervals. Peaks mixed with multiple components were separated using a commercial software package Spectra Cals (Galactic Industries). Through numerical fitting with a number of mixed Lorentzian and Gaussian line shapes of different widths and peak heights, the integrated intensity of the peak shapes could be calculated. Since the line widths of depolarized and polarized spectra do not differ appreciably at a given temperature, a simplification in the analysis of the data is possible by the simple measurements of peak height. These measured intensities over a wide range of incident angles were fit to eq 13 using the polynomial regression function in Sigmaplot, which resulted in three fitting parameters, $\langle P_{200}\rangle$, $\langle P_{400}\rangle$, and Raman tensor ratio, $r = \alpha'_{yy}/\alpha'_{zz}$. Details about fitting procedure are described elsewhere.[43]

Differentiation of band assignments between crystalline and amorphous regions was carried out by measuring the polarized Raman spectra of undrawn PLLA over the melting temperature (T_m). Temperature of the film was controlled using a hot stage (Linkam) that provides a relative accuracy in temperature of ±0.1 °C.

4. RESULTS AND DISCUSSION

4.1. Band Assignments. *4.1.1. Morphology Effect on Polarized Raman Spectra of PLLA.* Since amorphous regions in semicrystalline polymer coexist with crystalline regions,[44] the difficulty in analyzing the orientation of both amorphous and crystalline chain using polarized Raman spectra is the separation of morphology effect on the scattering intensity. If the crystallinity of a sample can be varied substantially as temperature

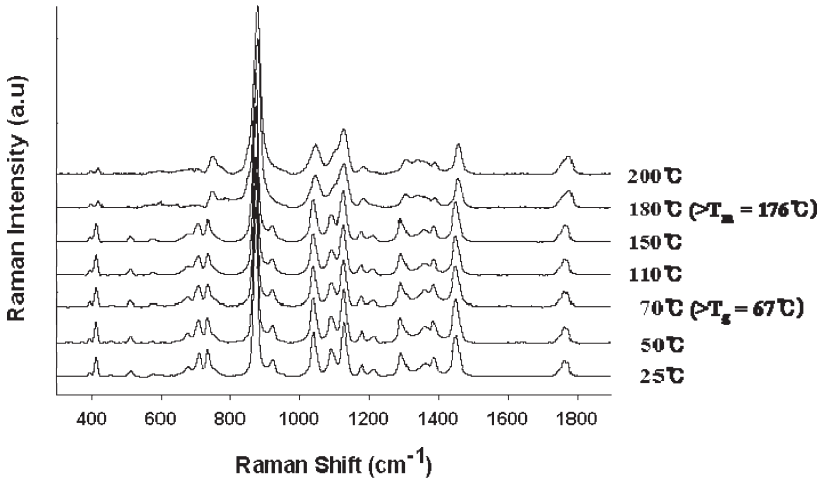

Figure 4. Polarized Raman spectra, $I_{\parallel}$, of undrawn PLLA at various temperatures.

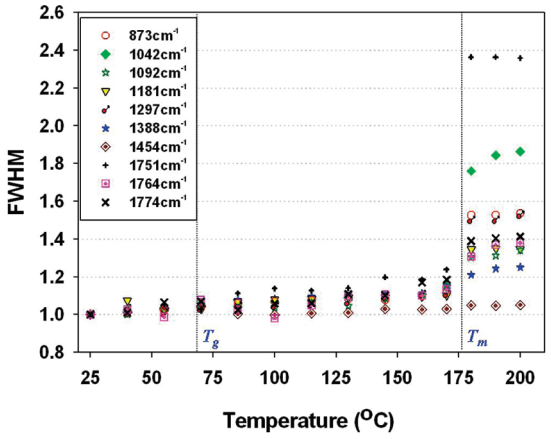

Figure 5. Temperature evolution of full width at half-maximum (fwhm) of various Raman bands normalized to the width of each band at 25 °C.

changes, it should be possible to assign some peaks to the crystalline chains by heat treatments. Thus, in order to evaluate the contributions of the crystalline and amorphous regions to peak intensities, polarized Raman spectra of isotropic crystalline PLLA film was measured at various temperatures from 25 to 200 °C at which the crystalline phase effect can be eliminated since the melting temperature of PLLA with α-helix form is known to be 175 °C.[45]

Figure 4 presents the peak changes in detail over the frequency regions studied as temperature changes. The changes of spectra at various temperatures provide information about morphology effects on the Raman activity for each band of PLLA. It is clearly seen that the peaks at 520, 708, and 919 cm^{-1} disappear after temperature reaches above T_m. This indicates these peaks are assigned to the vibration modes in long stereoregular chain segments and are usually absent from the spectrum of the molten PLLA. This agrees with the result of previous studies that bands at these frequencies are attributed only or mostly to the vibrations of chains in a crystalline region.[6,22,46] Thus, it is possible to identify orientation of scattering units in crystalline phases by analyzing Raman scattered intensity of these bands.[22]

However, other peaks are present in the melt, and they must be the result of the overlap of peaks belonging to each of the two phases. The contribution of the crystalline and amorphous phases to peak intensity can be roughly estimated from the changes of the full width at half-maximum (fwhm) of peaks with increasing temperature as shown in Figure 5. Increase of fwhm occurs when the chain conformation changes from well-defined order states to random states. It is because the structure of disordered chains encompasses a broad distribution of chain conformation, and thus their vibrational transitions have broad bandwidth. There are two features of interest in Figure 5: first, there is relatively slow increase of fwhm ratio with temperature up to melting temperature, followed by a sharp increase to a constant value, where the sharp increase was interpreted as occurring at the order−disorder phase transition. The slow broadening of peak width under T_m corresponds that a broad distribution of chain conformation without order−disorder phase transition occurring as temperature increases.

Therefore, the degree of change of fwhm gives qualitative information about how the morphology contributes to the peak intensity. For instance, the increase of fwhm of the peak at 1751 cm^{-1} becomes even greater at T_m than that of the 1454 cm^{-1} peak. With these comparisons, it is plausible to conclude that the assigned band at 1751 cm^{-1} is significantly related to the chain vibration in amorphous regions. Little change of bandwidth at 1454 cm^{-1} even at the temperatures above T_m may indicate that the shape of the peak is not dominated by the vibrations of crystalline chains and does not change much over T_m due to disappearance of crystalline phase. For other bands, each has different degrees of fwhm changes as a function of temperature, which indicates each band may have different contribution from both phases.

4.1.2. Raman Tensor Form and Symmetry of Vibration. As the forgoing discussion illustrates, it is necessary to determine the form of Raman tensor prior to the study of orientation of scattering units by measuring depolarization ratio in isotropic state, R_{iso}. Since it has been known that PLLA has α-helix structure,[44,47] and the structure is also likely to be preserved in the amorphous regions, the tensor forms were classified into two symmetry types, A- and E-mode.[20,31] In addition, we assume that any deformation in our study does not affect the helical structure of PLLA since the peak at 919 cm^{-1}, which reflects 10_3 helix structure,[46] does not shift under the deformation.

Figure 6 shows the measured polarized Raman spectra of an undrawn PLLA film and deconvolution of mixed peaks.

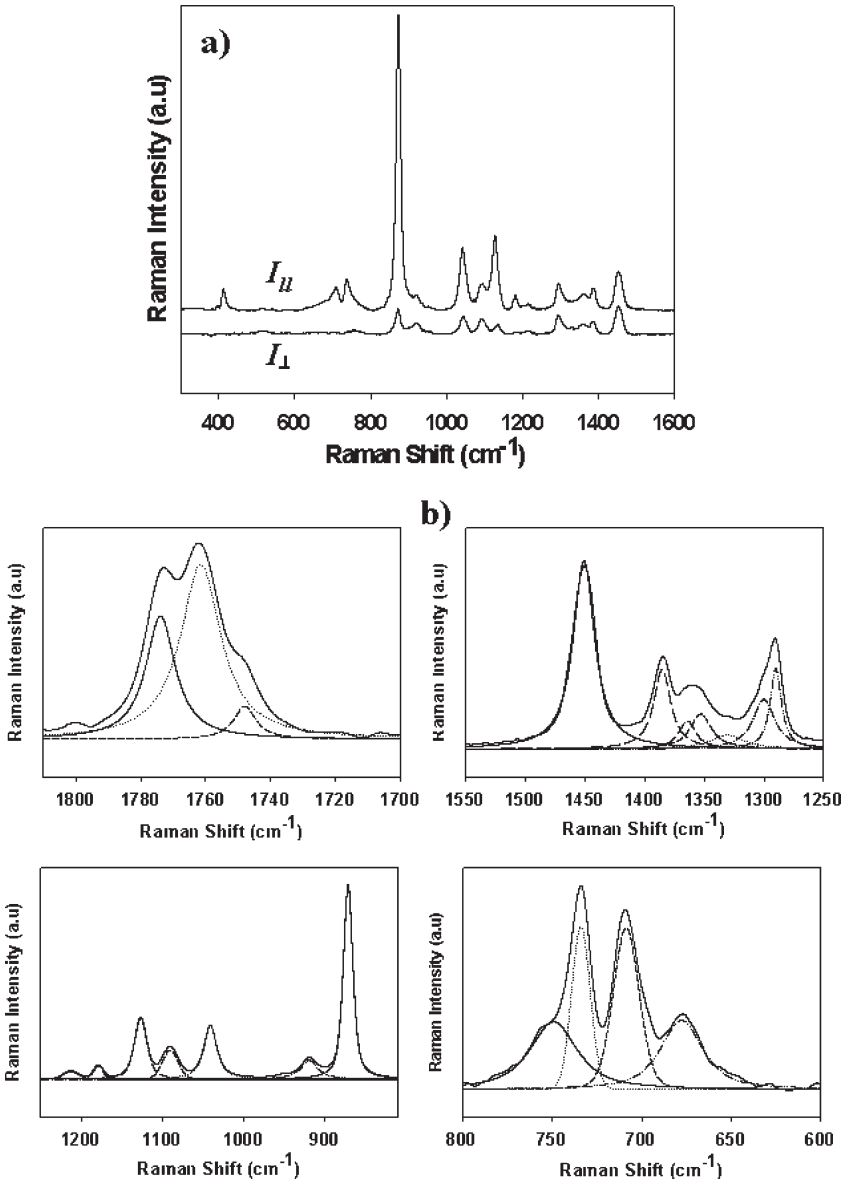

Figure 6. Polarized Raman spectra of isotropic crystalline PLLA measured at room temperature: (a) $I_{\parallel}$ and $I_{\perp}$; (b) decomposition of spectra over the range from 600 to 1800 cm^{-1}.

According to R_{iso} values of each band, the tensor form is classified to A-mode if R_{iso} is smaller than 0.75. In this case, the off-diagonal components of the Raman tensor are zero. If the R_{iso} value equals 0.75, on the other hand, the Raman band is an E-mode, in which case the diagonal components of the Raman tensor are zero. Band assignments and morphology effects on the major bands are based on published Raman results on PLLA[6,22,46,48] and are tabulated in Table 1. It is noteworthy that A-mode Raman bands are appropriate to quantify the "axial" ordering with simplified expression of the ODF. However, if one considers the E-mode, the coefficients will have to be calculated using nonsimplified expression for the ODF.

4.2. Orientation of the Principal Axis of Raman Tensor. *4.2.1. Angular Dependence of Polarized Raman Intensity.* All peaks attributed to each band were analyzed over the whole range of rotating angle in detail, and the intensity profiles for the four peaks as a function of rotating angle, θ, are shown in Figure 7. The pattern of 2-fold and 4-fold rotational symmetry of $I_{\parallel}(\theta)$ and $I_{\perp}(\theta)$ is conformable to trigonometric periodicities of expansion in eq 7. Interesting observation is that there are four types of angular dependence of $I_{\parallel}$ which are very similar to four types of orientation distribution functions as described in section 2.4.

The pattern of intensity profile of peak at 1388 cm^{-1} has a single maximum at θ =0° and monotonically decreases until θ = 90°. The intensity of peak at 1092 and 1454 cm^{-1} monotonically increases as the rotating angle increases and has a single maximum at 90°. A unimodal intensity profile is seen for the bands at 919 cm^{-1}. Angular dependence of Raman intensities of the other bands such as 873 cm^{-1} band appear to be bimodal having two maxima at θ = 0° and 90° and one minimum at specific angle when the film is deformed such that λ = 4. Herein it is important to differentiate polar angle β from the rotating angle, θ. The intensity profiles are constructed as a function of the rotating angle, θ and the plots of orientation distribution are made as a function of polar angle β.

dx.doi.org/10.1021/ma101553v |*Macromolecules* 2011, 44, 2120–2131

Table 1. Raman Band Assignments and Morphology Effects on the Peak[a]

Raman shift (cm^{-1})	morphology effect	R_{iso}	bands assignments
398M−411M	Cr/Am	0.721−0.152	δCCO
520w	Cr	/	δC−CH3+ δCCO
708M	Cr ≫ Am	0.089	γC═O
736M	Cr/Am	0.062	δC═O
873VS	Cr/Am	0.095	νC−COO
919M	Cr	0.841	rCH3 + ν
1042S	Am > Cr	0.267	νC−CH3
1092S	Cr/Am	0.501	ν(COC)s
1128S	Cr/Am	0.109	r(CH3)as
1181M	Cr/Am	0.086	ν(COC)as + r(CH3)as
1297M	Cr/Am	0.577	δCH
1388M	Cr > Am	0.673	δ(CH3)s
1454S	Cr > Am	0.741	δ(CH3)as
1751M	Am ≫ Cr	0.463	νC═O
1764M−1774M	Cr/Am	0.182−0.146	

[a] VS = very strong; S = strong; M = medium; w = weak; s = symmetric; as = asymmetric, Cr: crystalline chain, Am: amorphous chain, A > B: more attribution to A rather than B, A ≫ B: even more attribution to A rather than B, Cr/Am: mixed attribution to both phase but portion of effect from morphology is not definitive, /: difficult to decide.

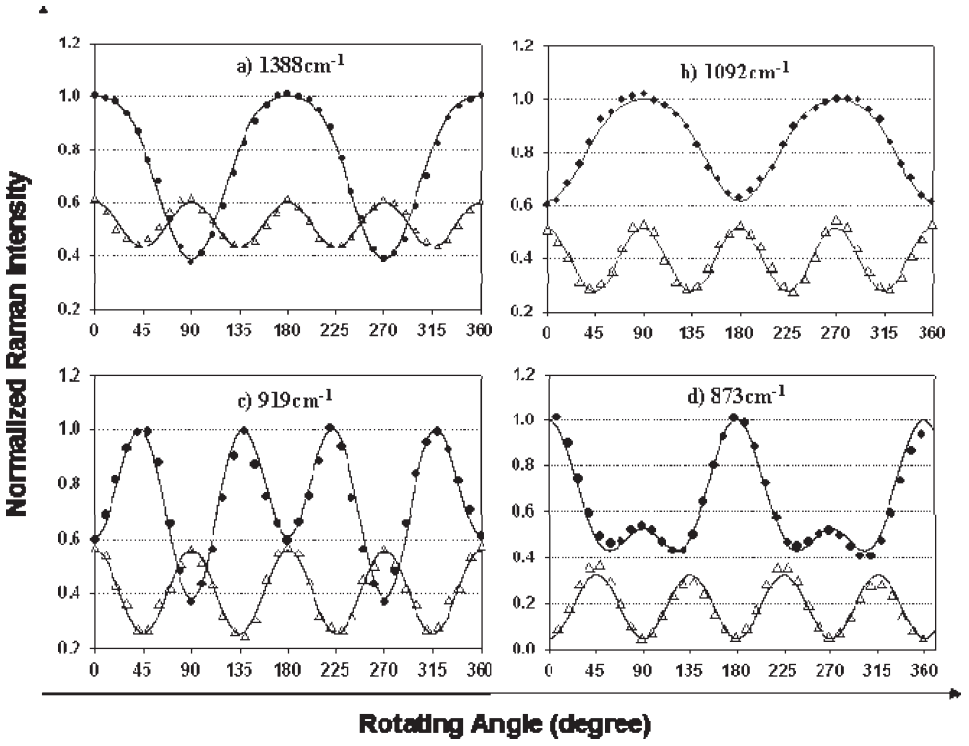

Figure 7. Angular dependence of polarized Raman intensities of stretched film ($\lambda = 4$): (●) measured $I_{\parallel}$, (Δ) measured $I_{\perp}$, and solid lines are their fitting results. (a) Monotonic decrease of $I_{\parallel}$ for band at 1388 cm^{-1}. (b) Monotonic increase of $I_{\parallel}$ for band at 1092 cm^{-1}. (c) Unimodal shape of $I_{\parallel}$ for band at 919 cm^{-1}. (d) Bimodal shape of $I_{\parallel}$ for band at 873 cm^{-1}.

Since the pattern of the intensity profile follows different ODF types, experimentally obtained intensity profiles at different draw ratios are fitted to the ODF models of Nomura et al.,[38] and fitting results as a function of draw ratios are presented in Figure 8. From Figure 8, we can see significant changes of the shape of intensity profiles under the deformation of films. In previous works about uniaxially drawn PLLA,[22,49] the pseudoaffine deformation model[50] was proposed for the deformation of molecular chain in the amorphous regions while the degree of crystalline orientation increases slowly at low draw (or stretch) ratios followed by a rapid rise as a result of crystal rotation and slip along the stretching direction at high drawing ratio.

This proposed deformation mechanism accounts for the variation of intensity profile with various stretch ratios based on knowledge about morphology contribution to the peak intensity qualitatively concluded in Table 1. In the case of the bands at 1092,

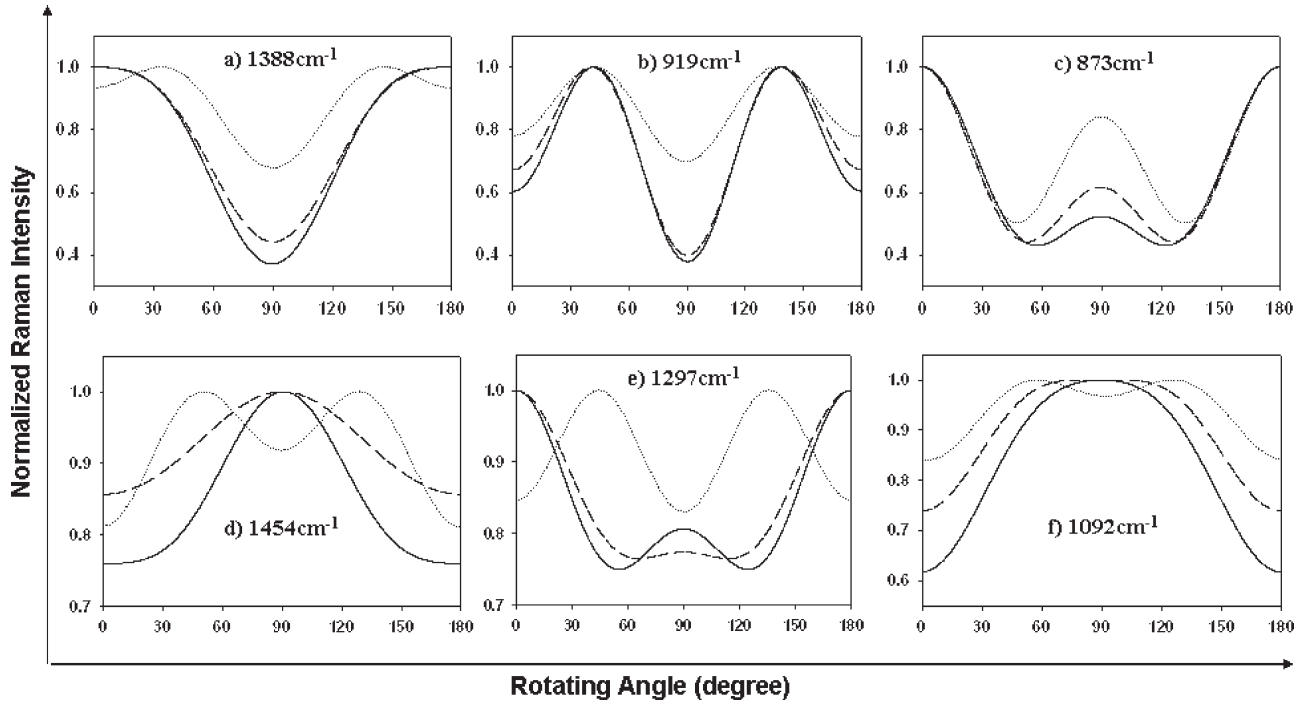

Figure 8. Angular dependence of $I_{\|}$ for various bands at different stretch ratios: dotted line is fitting result of $I_{\|}(\theta)$ at $\lambda = 2$, medium−medium line is fitting result of $I_{\|}(\theta)$ at $\lambda = 3$, and solid line is fitting result of $I_{\|}(\theta)$ at $\lambda = 4$.

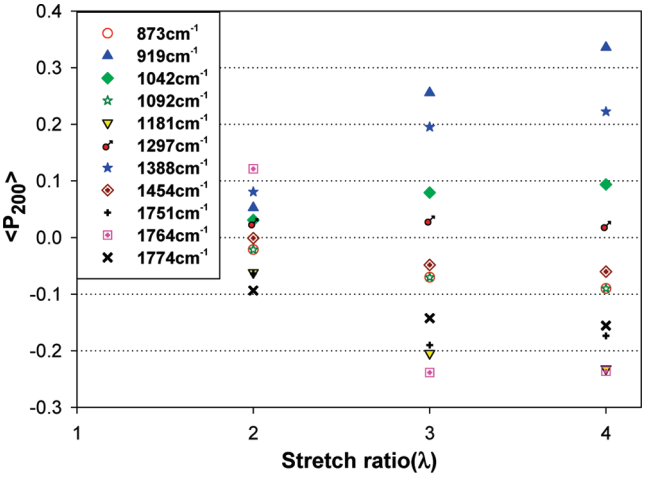

Figure 9. Plots of calculated values of $\langle P_{200}\rangle$ of vibration bands as a function of stretch ratio.

1297, and 1454 cm^{-1}, for instance, Raman peaks are attributed to the vibration of chains both in the crystalline region and in the amorphous region. This mixed contribution of morphology to peak intensity can explain the difference in intensity profiles according to stretch ratios in Figure 8. For the above three Raman bands in Figure 8, Figure 8 shows remarkable changes of profile shape when stretch ratio changes from $\lambda = 2$ into $\lambda = 3$, but profile shape is more or less the same between $\lambda = 3$ and $\lambda = 4$. This suggests that scattering units in both the amorphous part and the crystalline part are involved in the orientation process while the sample is being deformed to low stretch ratio ($\lambda = 2$). However, at high stretch ratio, $\lambda > 2$, the crystal orientation increases dramatically and then levels off due to the essentially complete microfibrillar transformation, and any further increase in orientation is confined to the amorphous regions. Thus, it results in the change of profile shape.

This approach is interpreted as evidence for a clear segregation of the crystalline and amorphous phases. Additional evidence is shown in the intensity profile of the crystalline peak at 919 cm^{-1}, where angular dependence of peak intensity increases abruptly from $\lambda = 2$ to $\lambda = 3$, but it almost level off at higher stretch ratios. These behaviors are in accord with previous results.[22,49]

With the profile changes at other peaks, however, it is difficult to explain the deformation mechanism of PLLA because angular dependence of the peak intensity is dependent on not only the mixed contribution of morphology but also the arbitrary angle of tilt that the symmetry axis makes against molecular chain axis.

4.2.2. $\langle P_{200}\rangle$ and $\langle P_{400}\rangle$ of the Principal Axis of Raman Tensors. Depolarization ratios, $R(\theta)$, for each band were obtained with experimental measurement of $I_{\|}(\theta)$ and $I_{\perp}(\theta)$. Orientation order parameters of the principal axis of Raman tensor, $\langle P_{200}\rangle$ and $\langle P_{400}\rangle$, and Raman tensor ratio, $r = \alpha'_{yy}/\alpha'_{zz}$, were calculated as a result of fitting measured data to eq 13. Obtained $\langle P_{200}\rangle$ is plotted against stretch ratios in Figure 9. It was observed that the $\langle P_{200}\rangle$ values for Raman bands at 919, 1042, 1297, and 1388 cm^{-1} increase positively as the stretch ratio becomes high; this implies the measured axis of symmetry has a tendency to align toward the drawing direction. In contrast, a decreasing $\langle P_{200}\rangle$ value toward negative says that orientation direction of symmetry axis becomes far away from uniaxially drawn direction beyond 45°. As seen in Figure 9, decreasing $\langle P_{200}\rangle$ values for bands at 1751−1764−1774 cm^{-1} with increasing stretch ratio imply that the molecular chains orient toward the drawing direction since the C═O stretching vibration is thought to occur in a direction perpendicular to the polymer backbone.

Interesting information on the shape of the ODF comes from the relation between $\langle P_{200}\rangle$ and $\langle P_{400}\rangle$ of the principal axis of

dx.doi.org/10.1021/ma101553v |*Macromolecules* 2011, 44, 2120–2131

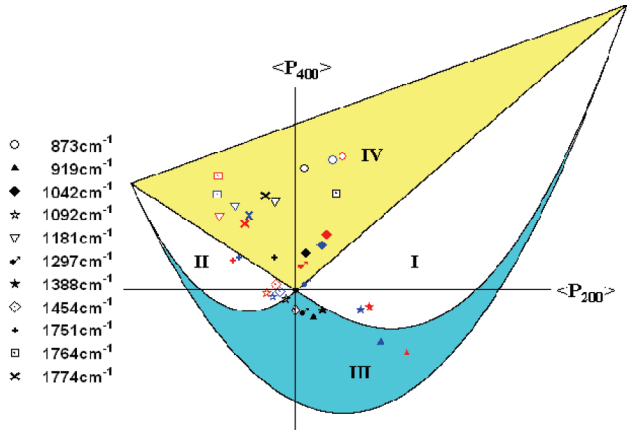

Figure 10. Plots of $\langle P_{400}\rangle$ against $\langle P_{200}\rangle$ calculated from fitting measured intensities to eq 13 for various vibration bands: each mark corresponds to each Raman band, and different colors with same mark indicate the values obtained at different stretch ratios (black ones at λ = 2, blue ones at λ = 3, and red ones at λ = 4).

Raman tensor. $\langle P_{200}\rangle$ and $\langle P_{400}\rangle$ values obtained for each Raman band are plotted in the P_2P_4 plane which is theoretically limited by Nomura et al.[38] and Bower[39] in Figure 10. They classified four domains where mutual relationship between $\langle P_{200}\rangle$ and $\langle P_{400}\rangle$ should be limited according to the four types of ODF. We can clearly see that the $\langle P_{200}\rangle$ and $\langle P_{400}\rangle$ values of each band are divided to be well inside each domain; values for 1388 cm^{-1} in domain I, those for 1092 cm^{-1} in domain II, value for 919 cm^{-1} in domain III, and those for other frequencies in domain IV.

These results are consistent with the matches between the profile shapes of $I_{\|}(\theta)$ and those of ODF as shown in Figures 8 and 2, respectively. It is more clearly seen in the case of 1297 cm^{-1} for which $\langle P_{200}\rangle$ and $\langle P_{400}\rangle$ ranges from domain III to domain IV as stretch ratio increases. As shown in Figure 8, the pattern of $I_{\|}(\theta)$ of this peak varies from unimodal to bimodal function, which is thought for the type of ODF to change in the same way. Thus, values of $\langle P_{200}\rangle$ and $\langle P_{400}\rangle$ at λ = 3 and λ = 4 are supposed to be in domain IV, whereas those of $\langle P_{200}\rangle$ and $\langle P_{400}\rangle$ at λ = 2 remain in domain III. The same explanation can be applied to the case of the Raman band at 1454 cm^{-1}. The Raman band at 1454 cm^{-1} is assigned to CH_3 asymmetric deformation modes, and CH_3 groups in PLLA are perpendicular to the molecular chain. Assuming that the Raman tensor is oriented along the direction of the CH_3 bond, our results show that the molecular chains are oriented along the deformation direction with a Gaussian distribution at high stretch ratio (refer to Figure 8). Therefore, we are able to predict the approximate pattern of ODF of polymer chains by measuring the intensity profile as a function of sample rotating angle.

However, it does not necessarily mean that these derived values of $\langle P_{200}\rangle$ and $\langle P_{400}\rangle$ reflect accurately the ODFs of polymer chains in the amorphous and crystalline region, respectively. This is because the analyzed scatterings have contributions from both phases, of which polymer chains respond differently to macroscopic deformation. Consequently, ODFs of the principal axis of Raman tensors averaged over both phases have a unimodal or bimodal function although the ODF of chains in each phase in fact may change monotonically. Furthermore, the tilt angle, Ψ, between the symmetry axis of Raman tensor and the helix axis should be considered to calculate ODF of molecular chains unless $\psi = \pm n\pi$, $n = 0, \pm1, \pm2, \ldots$.

From the above discussion, we propose that plotting the intensity profiles, $I_{\|}(\theta)$, of Raman scattering of certain selected bands can provide valuable information about the response of amorphous and crystalline chains separately under the deformation if the band is attributed to only one phase and the symmetry axis of Raman tensor is collinear with chain backbone axis.

4.3. Orientation of Amorphous Polymer Chains. *4.3.1. Orientation of Amorphous Polymer Chain.* Since the orientation information on crystalline chains in PLLA can be obtained using X-ray diffraction,[22] we would focus on discussing the orientation of amorphous chains in PLLA under deformation. Basic information for quantifying the degree of orientation of crystalline parts is briefly discussed in the Supporting Information.

As discussed above, experimentally obtained $\langle P_{200}\rangle$ and $\langle P_{400}\rangle$ values represent the orientation distribution of the principal axis of the Raman tensor in a given coordinate system. In order to quantify the orientation degree of chains in the amorphous region, not only the contribution of vibration in both amorphous and crystalline chains to Raman peak should be separated but also the tilting angle, Ψ, should be considered.

Although morphology effect on Raman intensity was qualitatively approximated based on the variations of Raman bandwidth according to the temperature, exact quantification is still unclear. Moreover, an accurate knowledge of Ψ is quite complicated, perhaps impossible, only with analysis of experimentally measured Raman spectra unless quantum mechanical calculations of polarizability change during vibration are carried out in parallel.

Tanaka et al. reported an elegant approach to obtain the tilt angle Ψ by combining $\langle P_{200}\rangle$ and $\langle P_{400}\rangle$ for the cylindrical symmetry axis of Raman tensor with those from wide-angle X-ray diffraction (WAXRD) and birefringence measurement.[21,22] Once the tilt angle, Ψ, has been determined, the orientational order parameters of amorphous chains, $\langle P_{200}\rangle_{amorphous}$, were obtained from $\langle P_{200}\rangle$ for the Raman band which is contributed from both crystalline and amorphous phase. $\langle P_{200}\rangle_{amorphous}$ was calculated from eq 15 with the knowledge of the degree of crystallinity, χ_c, and sample birefringence, Δn.[22,51,52]

$$\Delta n = \chi_c\langle P_{200,c}\rangle\Delta n_c + (1-\chi_c)\langle P_{200,a}\rangle\Delta n_a \qquad (15)$$

Herein lies the difficulty of decoding the individual contributions from the amorphous and crystalline regions. This equation can be applied for separating the orientation degree of amorphous and crystalline chains from the averaged values if the contribution of vibration of chains in amorphous and crystalline regions to Raman intensity is equal. Although qualitative separation of the contribution of morphology to Raman intensity is possible as shown in the discussion dealing with the fwhm in Figure 5, quantifying those exactly is quite difficult and not obvious. It would be quite useful to be able to figure out how to separate these contributions both qualitatively and, more importantly, quantitatively and merits further attention.

Free from the degree of contribution, the band at 1751 cm^{-1} may be used for the orientation of amorphous chains. It can be assumed that the contribution of crystalline chains to the peak intensity of band at 1751 cm^{-1} is so small that it can be ignored. In addition, the depolarization ratio, 0.463, obtained for this band of the unstretched sample is again an indication that the band is symmetric, and hence a good approximation to simple ODF will be valid to apply eq 13. However, we were not able to obtain the orientational order parameters of amorphous chains due to the lack of tilting angle for the Raman band at 1751 cm^{-1}. Although the direction of transition moment of νC═O(ester) was reported to be tilted about 53 ± 3° from the molecular chain axis in α-helix system,[53] using this information may also product another

assumption. Thus, rather than obtaining exact values of orientation degree for amorphous chains, what we propose is a new way to analyze polarized Raman spectra to characterize anisotropic behavior of semicrystalline chains under deformations.

5. CONCLUSIONS

The complex behavior of chain orientation in the semicrystalline PLLA system was studied by means of polarized Raman spectroscopy. The present paper employed a simple approach to the use of polarized Raman, which seeks to provide additional information on the orientation distribution from examining the complete range of orientation of the symmetry axis of Raman tensor in relation to the polarization directions. The measurements of the angular dependencies of the scattered intensity of assignable vibration bands, $I_{\perp}(\theta)$ and $I_{\parallel}(\theta)$, were performed to determine the orientation order parameters of scattering units. Comparison of calculated values, $\langle P_{200}\rangle$ and $\langle P_{400}\rangle$, with predicted ones was made according to types of ODF, and the results suggest that measurement of polarization of scattered intensity as a function of rotating angle can allow the orientation distribution function to be determined with good accuracy without the use of information entropy theory.

In order to characterize the orientation degree of crystalline chains and amorphous chains separately, we assigned Raman bands according to the effect of morphology on Raman intensity of the bands. The peak at 1751 cm^{-1} was mostly attributed to amorphous chain and could be directly used to obtain the orientation degree of amorphous chains. The molecular orientation distribution in the amorphous regions can be determined if the tilt angle, Ψ, is known. Using this approach, we found that most of the development of molecular orientation in the crystalline regions of uniaxially oriented PLLA film was complete after a stretch ratio of 3. The molecular orientation in the amorphous regions is much lower than that in the crystalline regions but seemed to be increase continually even after the molecular orientation in the crystalline regions was completed. These findings have implications for optimizing the recovery of semicrystalline polymers, as crystalline orientation generally is less recoverable compared to amorphous orientation. In turn, this finding has implications for optimization of the processes used to incorporate shape memory effects in such polymers.

■ ASSOCIATED CONTENT

Supporting Information. Wide-angle X-ray diffraction (WAXRD) data for the stretched films and quantification of orientation degree of crystalline chains as a function of stretching ratio. This material is available free of charge via the Internet at http://pubs.acs.org.

■ AUTHOR INFORMATION

Corresponding Author

*E-mail: assubbu@ntu.edu.sg (S.S.V.); mohan@mse.gatech.edu (M.S.).

■ ACKNOWLEDGMENT

This research was supported, in part, by the Office of Basic Energy Sciences, Department of Energy, Grant No. DESC0001412 and by an NSF grant-DMR-0706235.

■ REFERENCES

(1) Freed, L. E.; Marquis, J. C.; Nohria, A.; Emmanual, J.; Mikos, A. G.; Langer, R. *J. Biomed. Mater. Res.* **1993**, *27*, 11.
(2) Spenlehauer, G.; Vert, M.; Benoit, J. P.; Boddaert, A. *Biomaterials* **1989**, *10*, 557.
(3) Martin, O.; Averous, L. *Polymer* **2001**, *42*, 6209.
(4) Kulinski, Z.; Piorkowska, E. *Polymer* **2005**, *46*, 10290.
(5) Reeve, M. S.; McCarthy, S. P.; Downey, M. J.; Gross, R. A. *Macromolecules* **1994**, *27*, 825.
(6) Smith, P. B.; Leugers, A.; Kang, S. H.; Hsu, S. L.; Yang, X. Z. *J. Appl. Polym. Sci.* **2001**, *82*, 2497.
(7) Okuzaki, H.; Kubota, I.; Kunugi, T. *J. Polym. Sci., Part B: Polym. Phys.* **1999**, *37*, 991.
(8) Furuhashi, Y.; Kimura, Y.; Yoshie, N.; Yamane, H. *Polymer* **2006**, *47*, 5965.
(9) Gibson, A. G.; Davies, G. R.; Ward, I. M. *Polymer* **1978**, *19*, 683.
(10) Murthy, N. S.; Minor, H.; Bednarczyk, C.; Krimm, S. *Macromolecules* **1993**, *26*, 1712.
(11) Venkatraman, S. S.; Tan, L. P.; Joso, J. F. D.; Boey, Y. C. F.; Wang, X. T. *Biomaterials* **2006**, *27*, 1573.
(12) Venkatraman, S. S.; Boey, F. Polymeric stent and method of manufacture. U.S. Patent 2005/0021131, Jan 27, 2005.
(13) Wong, Y. S.; Xiong, Y.; Venkatraman, S. S.; Boey, F. Y. C. *J. Biomater. Sci., Polym. Ed.* **2008**, *19*, 175.
(14) Bower, D. I.; Maddams, W. F. *The Vibrational Spectroscopy of Polymers*; Cambridge University Press: Cambridge, 1989; pp 107−161.
(15) Cunningh, A.; Ward, I. M.; Willis, H. A.; Zichy, V. *Polymer* **1974**, *15*, 749.
(16) Bower, D. I. *J. Polym. Sci., Part B: Polym. Phys.* **1972**, *10*, 2135.
(17) Maxfield, J.; Stein, R. S.; Chen, M. C. *J. Polym. Sci., Part B: Polym. Phys.* **1978**, *16*, 37.
(18) Robinson, M. E. R.; Bower, D. I.; Maddams, W. F. *J. Polym. Sci., Part B: Polym. Phys.* **1978**, *16*, 2115.
(19) Pigeon, M.; Prudhomme, R. E.; Pezolet, M. *Macromolecules* **1991**, *24*, 5687.
(20) Tanaka, M.; Young, R. J. *J. Macromol. Sci., Phys.* **2005**, *B44*, 967.
(21) Tanaka, M.; Young, R. J. *J. Mater. Sci.* **2006**, *41*, 963.
(22) Tanaka, M.; Young, R. J. *Macromolecules* **2006**, *39*, 3312.
(23) Ferraro, J. R.; Nakamoto, K.; Brown, C. W. *Introductory Raman Spectroscopy*, 2nd ed.; Academic Press: San Diego, 2003; pp 13−30.
(24) Ovander, L. N. *Opt. Spektrosk.* **1960**, *9*, 571.
(25) Roe, R. J.; Krigbaum, W. R. *J. Appl. Phys.* **1964**, *35*, 2215.
(26) Roe, R. J. *J. Polym. Sci., Part A-2: Polym. Phys.* **1970**, *8*, 1187.
(27) Long, D. A. *Raman Spectroscopy*; McGraw-Hill International Book Co.: New York, 1977; pp 41−73.
(28) Zannoni, C. On the Description of Ordering in Liquid Crystals. In *The Molecular Dynamics of Liquid Crystals*; Luckhurst, G. R., Veracini, C. A., Eds.; Kluwer Academic Publishers: Dordrecht, 1994; Chapter 2.
(29) Jen, S.; Clark, N. A.; Pershan, P. S.; Priestley, E. B. *J. Chem. Phys.* **1977**, *66*, 4635.
(30) Vangurp, M. *Colloid Polym. Sci.* **1995**, *273*, 607.
(31) Bower, D. I. *J. Phys. B: At. Mol. Opt. Phys.* **1976**, *9*, 3275.
(32) Jen, S.; Clark, N. A.; Pershan, P. S.; Priestle, E. B. *Phys. Rev. Lett.* **1973**, *31*, 1552.
(33) Miyano, K. *J. Chem. Phys.* **1978**, *69*, 4807.
(34) Purvis, J.; Bower, D. I. *J. Polym. Sci., Part B: Polym. Phys.* **1976**, *14*, 1461.
(35) Rousseau, M. E.; Lefevre, T.; Beaulieu, L.; Asakura, T.; Pezolet, M. *Biomacromolecules* **2004**, *5*, 2247.
(36) Jones, W. J.; Thomas, D. K.; Thomas, D. W.; Williams, G. *J. Mol. Struct.* **2004**, *708*, 145.
(37) Southern, C. D.; Gleeson, H. F. *Eur. Phys. J. E* **2007**, *24*, 119.
(38) Nomura, S.; Nakamura, N.; Kawai, H. *J. Polym. Sci., Part A-2: Polym. Phys. Ed.* **1971**, *9*, 407.
(39) Bower, D. I. *J. Polym. Sci., Part B: Polym. Phys.* **1981**, *19*, 93.
(40) Nomura, S.; Kawai, H.; Kimura, I.; Kagiyama, M. *J. Polym. Sci., Part A-2: Polym. Phys.* **1970**, *8*, 383.

(41) Born, M.; Wolf, E. *Principles of Optics*, 5th ed.; Pergamon Press Ltd.: Oxford, 1975.
(42) Mattoussi, H.; Srinivasarao, M.; Kaatz, P. G.; Berry, G. C. *Macromolecules* **1992**, *25*, 2860.
(43) Park, M. S.; Yoon, B.-J.; Park, J. O.; Prasad, V.; Kumar, S.; Srinivasarao, M. *Phys. Rev. Lett.* **2010**, *105*, 027801.
(44) Vasko, P. D.; Koenig, J. L. *Macromolecules* **1970**, *3*, 597.
(45) Hoogsteen, W.; Postema, A. R.; Pennings, A. J.; Tenbrinke, G.; Zugenmaier, P. *Macromolecules* **1990**, *23*, 634.
(46) Kister, G.; Cassanas, G.; Vert, M. *Polymer* **1998**, *39*, 267.
(47) Bailey, R. T.; Hyde, A. J.; Kim, J. J. *Spectrochim. Acta, Part A* **1974**, *A 30*, 91.
(48) Kister, G.; Cassanas, G.; Vert, M.; Pauvert, B.; Terol, A. *J. Raman Spectrosc.* **1995**, *26*, 307.
(49) Wong, Y. S.; Stachurski, Z. H.; Venkatraman, S. S. *Acta Mater.* **2008**, *56*, 5083.
(50) Ward, I. M. *Mechanical Properties of Solid Polymer*, 2nd ed.; John Wiley & Sons: New York, 1983.
(51) Stein, R. S.; Norris, F. H. *J. Polym. Sci.* **1956**, *21*, 381.
(52) Samuels, R. J. *J. Polym. Sci., Part A* **1965**, *3*, 1741.
(53) Tsuboi, M. *J. Polym. Sci.* **1962**, *59*, 139.